Journal of Functional Materials and Applied Engineering

Research Paper

Simultaneous removal of sulfamethoxazole and Cr(VI) from water by pulsed discharge plasma

Ingrid Larsen[1], Bjorn Nygaard[2], Chinedu Osazuwa[3,*]

[1] Department of Chemistry, University of Iowa, United States
[2] Department of Chemical Engineering, Faculty of Industrial Technology, Universitas Pembangunan Nasional "Veteran" Yogyakarta, Indonesia
[3] Bioresources Valorization Laboratory, Department of Chemical Engineering, Faculty of Engineering, University of Benin, Benin City, Edo State, Nigeria
*Corresponding author: IngridLarsen@uiowa.edu; Bjorn.Nygaard@gmail.com; ChineduOsazuwa@uniben.edu

Abstract. Real aquatic matrices are frequently burdened by intricate co-contamination from organic micropollutants and toxic heavy metals, creating an urgent demand for environmentally benign technologies capable of eliminating both contaminant classes in a single step. Pulsed discharge plasma (PDP) generates a cocktail of oxidative and reductive transient species that can concurrently oxidise organic compounds and reduce metallic ions. This study investigated the simultaneous PDP-driven degradation of sulfamethoxazole (SMX) and reduction of hexavalent chromium (Cr(VI)). The influences of electrical parameters, solution chemistry, and water-quality characteristics on the coupled removal efficiency were systematically evaluated. Maximal SMX elimination (50 mg·L^{-1}) was attained in the presence of 2 mg·L^{-1} Cr(VI), whereas optimal Cr(VI) reduction (0.7 mg·L^{-1}) was achieved upon spiking with 15 mg·L^{-1} SMX. Elevated applied voltage, pulse frequency, duty cycle, and gas-flow rate, together with acidic pH and low conductivity, markedly promoted the synchronous detoxification. Conversely, naturally occurring anions (Cl^-, HCO_3^-, SO_4^{2-}) and humic acid (HA) exerted inhibitory effects. Scavenger experiments confirmed that the formation and subsequent fate of hydroxyl radicals (·OH), superoxide radicals ($\cdot O_2^-$), singlet oxygen ($^1O_2$), hydrated electrons (e^-), and hydrogen atoms (·H) all played mechanistic roles in the dual-removal process. LC-MS and DFT analyses further enabled the proposal of three distinct SMX transformation pathways within the PDP system. Moreover, ECOSAR-based toxicity assessments indicated a substantial decrease in effluent ecotoxicity following treatment. Collectively, these findings establish PDP as a promising green technology for the concurrent abatement of antibiotic residues and toxic chromium from water.

Keywords: *plasma, composite wastewater, influencing factors, simultaneous removal, degradation pathways*

Received on 02 April 2025, Accepted on 25 April 2025, Published on 11 June 2025

1 Introduction

Over recent decades, China's rapid economic expansion has driven a marked escalation in industrial discharges. Effluents from sectors such as electrolysis, electroplating, papermaking, and textile dyeing are especially problematic, harbouring recalcitrant organics alongside highly toxic heavy metals [1]. Among these mixed contaminants, the co-occurrence of antibiotics and metallic pollutants has drawn mounting scientific concern because of their ubiquity and synergistic interactions [2]. Sulfamethoxazole (SMX), a representative sulfonamide antimicrobial widely administered against bacterial infections [3], resists environmental breakdown and can exert chronic ecological harm through bioaccumulation. Likewise, hexavalent chromium (Cr(VI)) ranks among the most prevalent and hazardous metallic pollutants; being non-biodegradable and acutely toxic, it poses severe threats to both drinking-water security and public health [4]. When SMX and Cr(VI) share the same aquatic compartment, their combined toxicity and enhanced mobility amplify risks to aquatic ecosystems and human populations [5]. Once released, these contaminants persist indefinitely, resisting natural attenuation and progressively concentrating up the food chain, thereby destabilising ecological equilibria and potentially eliciting teratogenic, carcinogenic, and mutagenic outcomes [6]. Furthermore, biological and abiotic processes can forge organometallic complexes that substantially heighten the overall toxicity of the wastewater matrix [7].

Conventional remediation of wastewater bearing both organic and metallic contaminants generally proceeds in two discrete stages: heavy metals are first stripped away via adsorption or chemical precipitation, and the residual organics are subsequently degraded through biological or oxidative treatments [8]. This sequential approach is inherently cumbersome, precluding the concurrent elimination of both pollutant classes while entailing elevated capital and operating costs and risking secondary contamination. Although photocatalysis has been proposed as a means of simultaneous treatment, its practical scale-up remains hampered by poor light-utilisation efficiency and the difficulty of recovering the catalyst [9]. Consequently, devising an efficient, environmentally benign technology capable of removing organic pollutants and Cr(VI) in a single step stands out as a pressing research imperative.

In recent years, non-thermal plasma (NTP) has emerged as a promising advanced oxidation technology for environmental cleanup [10]. NTP generates a rich cocktail of energetic species—including electrons, ions, excited-state atoms and molecules, and reactive free radicals—that supply the activation energy needed to drive reactions that would otherwise proceed slowly or not at all. Moreover, NTP offers straightforward implementation, superior treatment efficiency, and freedom from secondary contamination [11]. Pulsed discharge plasma (PDP), a subset of NTP, is distinguished by its dense population of high-energy electrons, elevated mean electron energy, and abundant production of reactive species, making it particularly attractive for aquatic pollutant remediation [12]. During operation, the high-energy electrons released in each discharge pulse strike water molecules, inducing excitation, dissociation, and ionization. These collisions are accompanied by physical phenomena such as ultraviolet emission, shock waves, and acoustic cavitation, alongside the generation of chemically active species. Oxidative transients such as hydroxyl radicals (·OH), atomic oxygen (O), and ozone (O_3) have been shown to rapidly mineralise organic contaminants in water [12–13]. Simultaneously, the discharge yields reductive species including hydrogen atoms (·H), hydrated electrons (e_aq^-), and hydrogen peroxide (H_2O_2). Notably, ·H is a potent reductant capable of converting aqueous Cr(VI) into the far less toxic Cr(III) [14]. Research has further demonstrated that the concurrent presence of ·OH and ·H creates a synergistic regime in which organic oxidation and metal reduction proceed in parallel [15]. Capitalising on this dual oxidative–reductive chemistry, the present investigation employs PDP technology to treat wastewater co-contaminated with organics and heavy metals, aiming to achieve simultaneous pollutant degradation and detoxification.

This paper discusses the feasibility of simultaneous removal of SMX and Cr(VI) by PDP. The effects of electrical parameters (input voltage, frequency, duty cycle), solution parameters (flow rate, initial pH, initial conductivity) and water quality parameters (Cl^-, HCO_3^-, SO_4^{2-}, HA) on the simultaneous removal effect were investigated. The effects of active species (·OH, $·O_2^-$, $^1O_2$, H_2O_2, e^-, ·H) on the simultaneous removal effect were investigated. Finally, the degradation pathway of SMX was inferred based on DFT theoretical calculations and relevant literature, and its toxicity was studied, thereby providing an important reference value for the simultaneous removal of organic pollutants and heavy metals from wastewater, alleviating the water environment crisis, and expanding the application range of low-temperature plasma water treatment technology.

2 Experimental section

2.1 Experimental setup

The built PDP composite wastewater treatment experimental platform is shown in Figure 1, mainly divided into an electrical detection system and an analysis and testing system. The experimental arrangement incorporates a pulse generator, a WFDBD plasma chamber, an oscilloscope, and paired high-voltage and current probes. The pulsed power unit runs on a nominal 220 V supply, covers an operating voltage span of 0–380 V, supports driving frequencies from 1 Hz up to 3 kHz, and permits continuous duty-cycle adjustment between 1 % and 100 %. The input voltage in the experiment was set to 140, 160, 180, and 200 V, and the discharge mode was corona discharge. Figure 2 shows the discharge image and discharge voltage and current waveforms of the reactor at an input voltage of 180 V. A peristaltic pump first feeds the composite wastewater into the upper inlet of the cylindrical DBD reactor. From the top-mounted ground electrode, the liquid descends along the external surface of the quartz inner tube as a film only a few micrometres thick, traverses the 9-mm annular gap between the outer mesh electrode and the inner tube, and is then recirculated continuously. At the same time, the solution

is detected by analytical instruments such as liquid chromatograph, spectrophotometer, and liquid chromatography–mass spectrometry.

Figure 1 Water treatment experimental platform

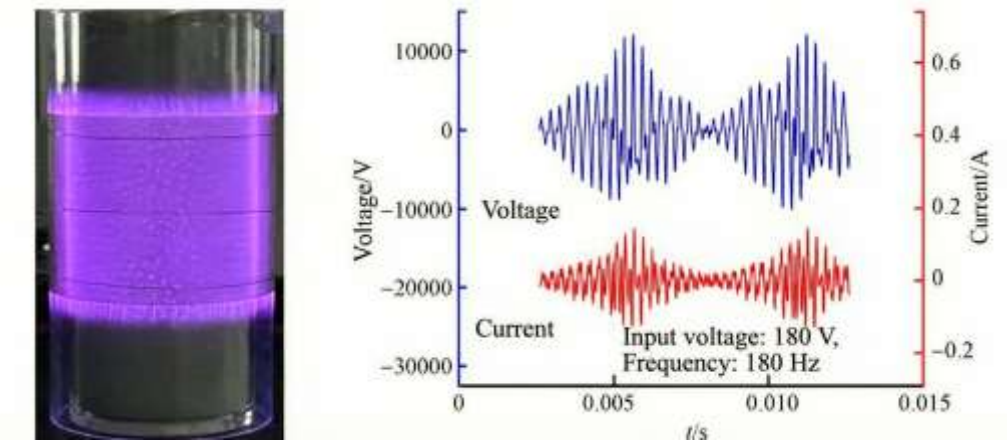

Figure 2 Discharge image and waveform of discharge voltage and current

2.2 Determination methods for SMX and Cr(VI) concentrations

Simultaneous abatement of SMX and Cr(VI) in the PDP system was evaluated using a 300 mL working volume over 30 min, with aliquots withdrawn every 5 min. In the first phase, electrical settings were held constant at 180 V input voltage, 180 Hz pulse frequency, 90 % duty cycle, 100 mL·min^{-1} flow rate, and neutral pH. With SMX fixed at 15 mg·L^{-1}, the influence of varying Cr(VI) levels on SMX decay was mapped; conversely, with Cr(VI) held at 2 mg·L^{-1}, the impact of changing SMX concentrations on Cr(VI) removal was assessed. In the second phase, both contaminants were maintained at 15 mg·L^{-1} SMX and 2 mg·L^{-1} Cr(VI) while electrical and solution parameters were systematically varied to probe their influence on the coupled treatment efficiency. When changing a certain parameter, other parameters remained unchanged (same as above). The SMX concentration was determined by liquid chromatography using a C18 column (5 μm, 4.6 mm × 250 mm), flow rate 1.0 mL·min^{-1}, detection wavelength 263 nm, mobile phase 50% water (0.1% phosphoric acid) and 50% methanol. The Cr(VI) concentration was detected by spectrophotometry. First, a color reagent was prepared by dissolving 0.20 g of diphenylcarbazide in 100 mL of 95% ethanol, and adding 400 mL of (1+9) sulfuric acid while stirring. Take 5 mL of water sample to 50 mL, add 2.5 mL of color reagent, mix well and let stand for 10 min for measurement, measured at λ = 540 nm.

The calculation methods for SMX degradation rate and Cr(VI) removal rate are shown in Equation (1):

$$\eta = [(C_0 - C_t)/C_0] \times 100\% \quad (1)$$

Where η is the SMX degradation rate or Cr(VI) removal rate, %; C_o is the initial concentration of SMX or Cr(VI), mg·L^{-1}; C_t is the concentration of SMX or Cr(VI) at treatment time t min, mg·L^{-1}. Plasma-driven mineralisation of dissolved organics follows first-order kinetics [16], whereas Cr(VI) attenuation obeys a pseudo-first-order rate law [17]. Therefore, the kinetics of SMX degradation and Cr(VI) removal were analyzed according to the first-order kinetic model, as shown in Equation (2):

$$\ln(C_0/C_t) = kt \quad (2)$$

Where C_o and C_t have the same definitions as in Equation (1); k is the reaction rate constant, min^{-1}; t is the treatment time, min.

2.3 Trapping agent experiments

To elucidate the role of plasma-derived reactive intermediates in driving SMX decomposition and Cr(VI) elimination, and to confirm the generation of free radicals within the discharge zone, a set of scavenger-based trapping assays was performed. Isopropanol (IPA), CCl_4, triethylenediamine (TEDA), p-benzoquinone (p-BQ) and HPO_4^{2-} were used to capture ·OH, ·H, $^1O_2$, $\cdot O_2^-$ and e^- respectively.

2.4 Density functional theory analysis method

Based on Gaussian 16 and Multiwfn software, B3LYP and M06 functionals were used to perform DFT calculations on SMX, including highest occupied molecular orbital (HOMO), lowest unoccupied molecular orbital (LUMO), and Fukui functions.

3 Results and discussion

3.1 Interaction between SMX and Cr(VI)

To ascertain whether Cr(VI) accelerates SMX breakdown within the WFDBD plasma reactor, its concentration was systematically varied; the outcomes are depicted in Figure 3a. The data reveal a non-monotonic trend: SMX elimination initially intensified with rising Cr(VI) levels, then subsided. Peak enhancement occurred at 2 mg·L^{-1} Cr(VI), where SMX degradation hit 88.6 %—a 13.0-percentage-point gain relative to the Cr(VI)-free control. This synergy arises because Cr(VI) sequesters electrons and hydrogen radicals during its reduction, sparing hydroxyl radicals that would otherwise be quenched by ·H and leaving more ·OH available to attack SMX. Yet, once Cr(VI) exceeded this optimum, its benefit waned: the Cr(III) formed was re-oxidized to Cr(VI), a process that competed with SMX for the limited oxidative species in solution, thereby lowering the overall degradation efficiency.

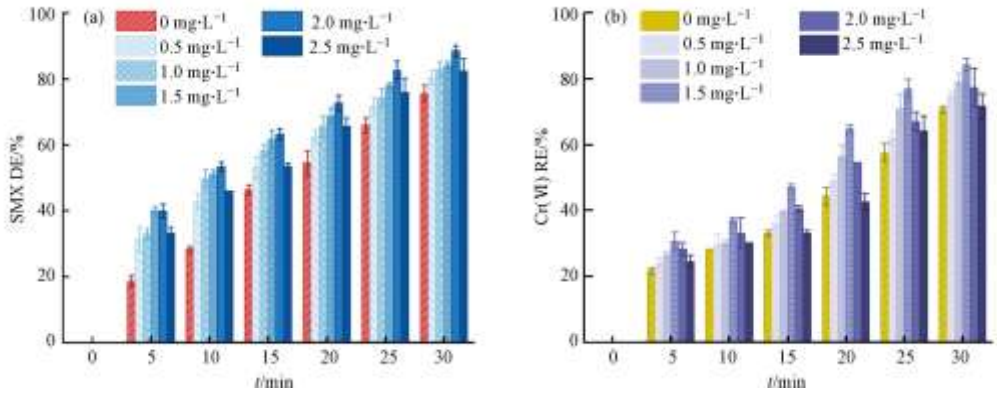

Figure 3 The interaction between SMX and Cr (Ⅵ): (a) the effect of Cr (Ⅵ) concentration on SMX degradation, (b) the effect of SMX concentration on Cr (Ⅵ) removal

Prior work has demonstrated that organic matter acting as a sacrificial agent can enhance heavy-metal-ion elimination [18]. Hence, to further probe the cooperative interaction between Cr(VI) and SMX, the influence of SMX concentration on Cr(VI) removal was examined. As illustrated in Figure 3b, Cr(VI) elimination first rose and then fell as SMX concentration increased. The optimum appeared at 15 mg·L^{-1} SMX, where Cr(VI) removal climbed from 70.8 % to 84.3 %. Evidently, SMX addition facilitated Cr(VI) reduction. During concurrent treatment, the presence of SMX furnished adequate reductive equivalents for Cr(VI) conversion. In the PDP environment, Cr(VI) → Cr(III) reduction and Cr(III) → Cr(VI) re-oxidation proceed simultaneously; by rapidly scavenging oxidants, SMX shifts the balance toward net reduction, thereby securing effective Cr(VI) detoxification. Nevertheless, an optimal SMX dosage exists: only at this level can dual-redox species such as H_2O_2 most efficiently drive Cr(VI) reduction. In summary, a pronounced synergistic interplay between SMX and Cr(VI) is operative within the PDP system.

3.2 Effects of electrical parameters

The input voltage affects the electric field strength between electrodes and determines the input energy of the reactor [19]. Raising the applied voltage elevates the discharge potential and, consequently, the discharge intensity [20].

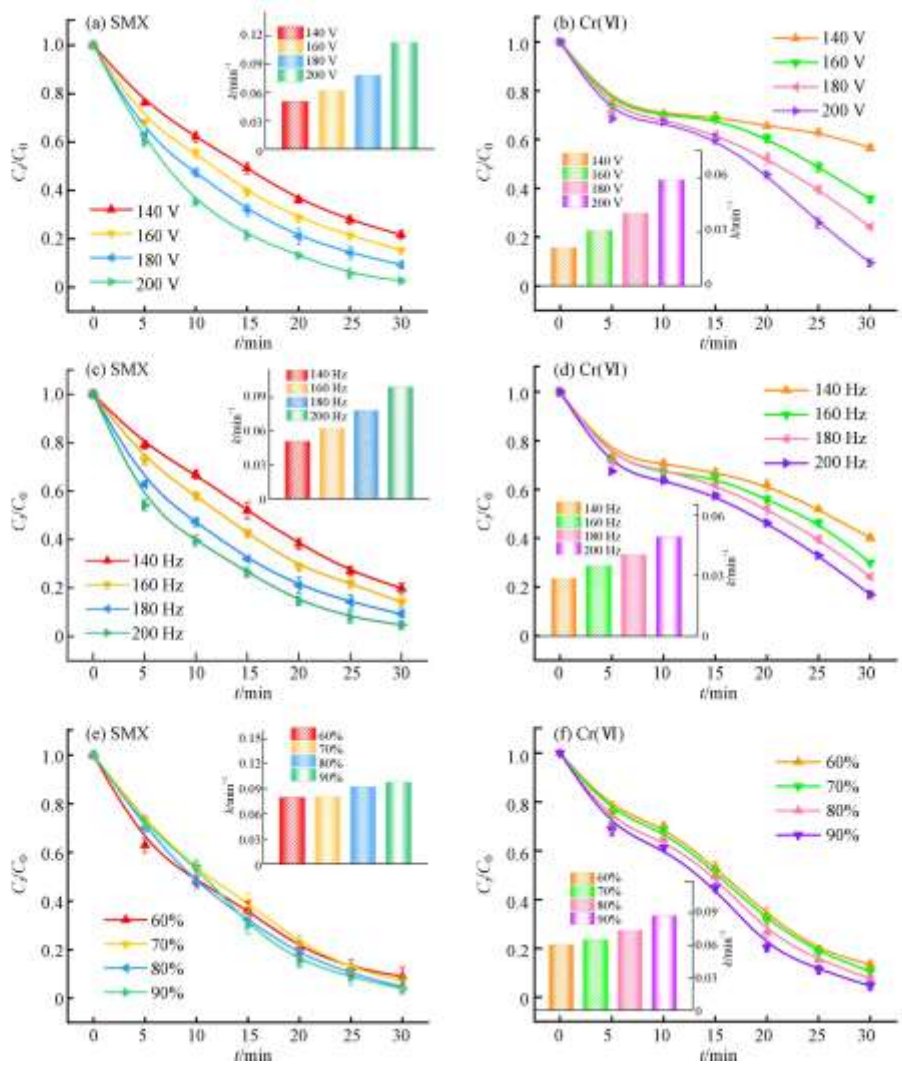

Figure 4 The influence of input voltage (a,b), frequency (c,d) and duty cycle (e,f) on SMX degradation and Cr (Ⅵ) removal

Simultaneously, UV emission, electron kinetic energy and velocity, together with the yield of reactive oxygen species and other transient active species, are all governed by the input voltage [21]. Against this backdrop, this segment examines how the applied voltage influences SMX degradation and Cr(VI) reduction. As depicted in Figures 4a–b, escalating the voltage progressively improved the elimination of both contaminants. At input voltages of 140, 160, 180 and 200 V (corresponding to discharge voltages of 11.2, 12.0, 13.0 and 14.0 kV), SMX degradation reached 78.4 %, 84.7 %, 90.7 % and 97.3 %, respectively, while Cr(VI) removal attained 44.4 %, 64.5 %, 75.8 % and 90.5 %. Likewise, the rate constants rose with voltage; at the highest setting they reached 0.113 min^{-1} for SMX and 0.059 min^{-1} for Cr(VI)—more than double the values recorded at 140 V. A higher voltage prompts the plasma to generate greater quantities of free radicals, ions, electrons and other active transients, wherein certain species drive organic oxidation while others mediate heavy-metal reduction [22]. Hence, increasing the voltage enhances the concurrent removal of both pollutants.

Pulse frequency is a pivotal operating parameter governing pollutant decomposition in PDP systems. Raising the pulse frequency amplifies discharge power, thereby fostering the production of reactive species [23]. To examine how frequency modulates SMX degradation and Cr(VI) reduction in water, replicate runs were carried out at 140, 160, 180 and 200 Hz while holding voltage constant. The data, compiled in Figures 4c–d, reveal that the elimination efficiencies for both SMX and Cr(VI) rose progressively with increasing frequency. At the upper limit of 200 Hz, maximal removal reached 95.3 % for SMX and 83.1 % for Cr(VI)—gains of 15.0 and 23.2 percentage points, respectively, over the 140 Hz baseline. Consistently, the associated kinetic constants also scaled upward with frequency. With the increase of frequency, the kinetic constant of SMX degradation gradually increased from 0.051 min^{-1} to 0.062, 0.078, and 0.099 min^{-1}, and the kinetic constant of Cr(VI) reduction increased from 0.028 min^{-1} to 0.034, 0.040, and 0.048 min^{-1}. As the frequency increases, higher concentrations of active substances are generated, and the concentration of residual pollutants in the aqueous solution decreases. In other words, the energy increases with frequency, resulting in higher degradation efficiency.

The duty cycle is also an important factor affecting the removal efficiency. Therefore, Figures 4e–f investigated the effect of duty cycle changes on the removal of SMX and Cr(VI). Although the SMX degradation curves partially overlapped, overall, the degradation effect was best when the duty cycle was 90%, reaching 96.1%, which was 5% higher than that at 60% duty cycle. Similarly, although the kinetic constant did not change significantly, it also gradually increased with the increase of duty cycle. Obviously, when the duty cycle increased from 60% to 70%, 80%, and 90%, the removal rate of Cr(VI) increased from 86.7% to 89.5%, 92.4%, and 99.9%. The duty cycle has a great influence on the discharge intensity. The luminous peak intensity at different duty cycles is different, which affects the generation of active substances and the removal of pollutants [24]. For example, as the duty cycle increases, although O_3 decay becomes faster, the peak level of O_3 in the reactor increases, making the oxidation effect of SMX better and better [25].

3.3 Effects of solution parameters

The solution flow rate affects the water film thickness, thereby affecting the formation of discharge and the diffusion of active species [23]. Figures 5a and 5b probe how the liquid flow rate modulates the concurrent SMX degradation and Cr(VI) reduction. For both processes, performance improves monotonically with increasing flow. As the circulation rate was stepped up from 40 to 60, 80, and 100 $mL \cdot min^{-1}$, the SMX elimination efficiency climbed from 92.9 % to 95.3 %, 96.1 %, and 96.8 % (Figure 5a), while Cr(VI) removal rose from 85.5 % to 89.5 %, 95.4 %, and 98.7 % (Figure 5b). Correspondingly, the pseudo-first-order rate constants for both contaminants increased with faster flow. This trend is attributed to the slightly thicker water film formed at higher flow rates, which narrows the discharge gap and thereby intensifies the plasma discharge [23]. In addition, the greater the flow rate, the more cycles, and the collision probability of pollutants and active substances (O_3, e^-, etc.) at the gas–liquid interface in the reaction zone increases, promoting SMX degradation and more effectively promoting Cr(VI) reduction.

Given that real wastewater matrices span a broad pH spectrum from acidic to alkaline, evaluating how the initial solution pH influences the elimination efficiencies of both SMX and Cr(VI) is essential. The change of pH showed

different results for the removal of the two, as shown in Figures 5c–d. Among them, the degradation effect of SMX was better under acidic and alkaline conditions, and slightly worse under neutral conditions. When pH was 2.99, 5.06, 6.83, 8.84, and 10.35, the SMX degradation rates were 90.9%, 87.6%, 82.4%, 86.4%, and 89.9%, respectively. The removal rate of Cr(VI) decreased with the increase of pH, and the effect was best under acidic conditions. When pH was 2.99, 5.06, 6.83, 8.84, and 10.35, the Cr(VI) removal rates were 96.9%, 85.4%, 68.9%, 60.8%, and 53.0%, respectively. When pH = 2.99, the removal rates of SMX and Cr(VI) were the highest, reaching 90.9% and 96.9%, respectively. Cr(VI) reacts with H_2O_2 to reduce to Cr(V), and further to Cr(IV) under acidic conditions. As shown in Equation (3), abundant H^+ (acidic medium) promotes the reduction of photogenerated electrons. When the pH value is higher than 5.0, the dominant species of Cr(VI) are CrO_4^{2-} or $Cr_2O_7^{2-}$, which require more H^+ to achieve the reduction of Cr(III) (Equations 4–5) [18].

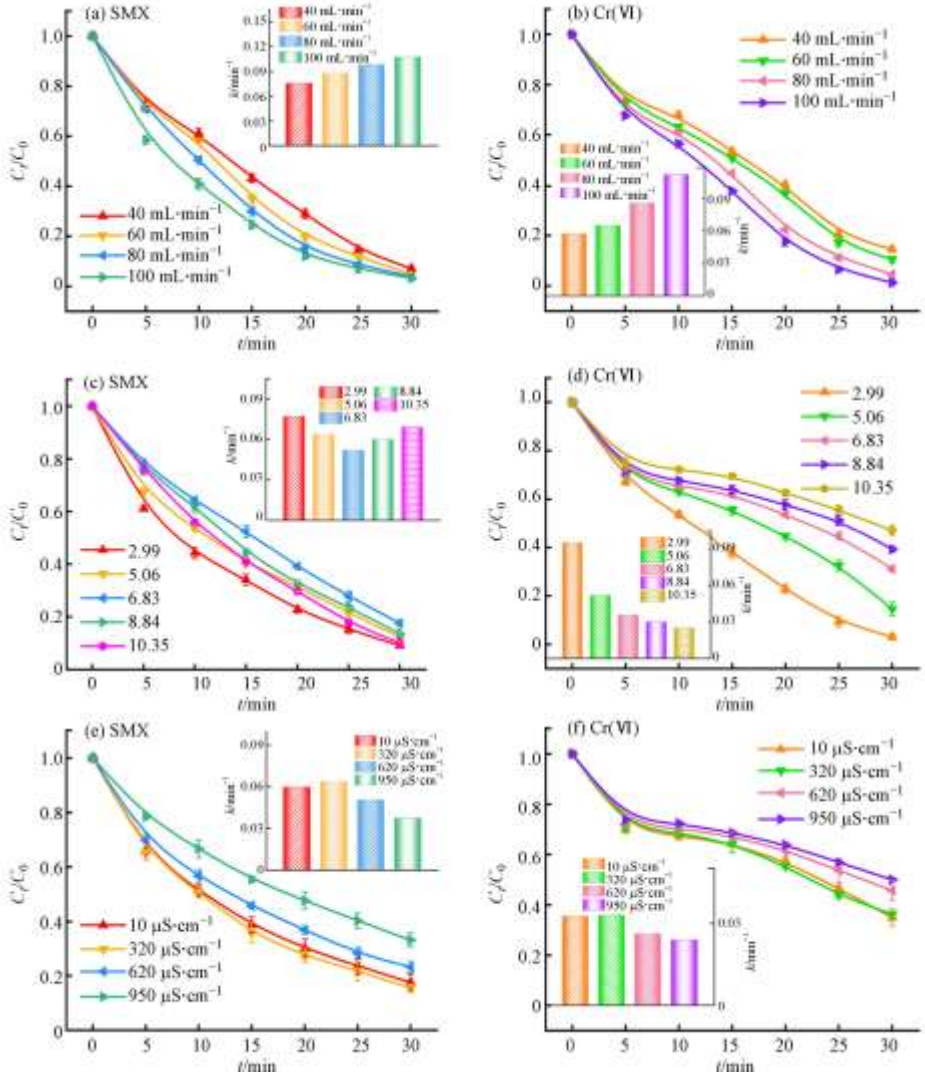

Figure 5 The influence of solution flow rate, solution initial pH initial and solution initial conductivity on SMX degradation and Cr (Ⅵ) removal

With the increase of acidity, the higher removal rate is attributed to the higher sensitivity of $HCrO_4^-$ to reduction than CrO_4^{2-}. Under acidic conditions, high concentrations of reactive oxygen species are generated, which is beneficial to the degradation of organic matter [26]. In addition to the better plasma removal effect under acidic conditions, the synergistic effect of SMX and Cr(VI) is also well reflected here.

$$HCrO_4^- + 7H^+ + 3e^- \rightarrow Cr^{3+} + 4H_2O \quad (3)$$

$$CrO_4^{2-} + 8H^+ + 3e^- \rightarrow Cr^{3+} + 4H_2O \quad (4)$$

$$2Cr_2O_7^{2-} + 16H^+ + 12e^- \rightarrow 4Cr^{3+} + 8H_2O + 3O_2 \quad (5)$$

Greater solution conductivity facilitates channel lengthening and discharge-current enhancement, which benefits plasma-induced SMX oxidation and Cr(VI) reduction. The impact of initial conductivity on the synchronous treatment was investigated in Figures 5e–f. Despite an overall downward trajectory for both SMX degradation and Cr(VI) removal as conductivity grew, the SMX decay rate showed a minor initial upswing—from 82.5 % to 84.5 %—as the starting conductivity was raised from 10 μS·cm^{-1} toward 320 μS·cm^{-1}. When the conductivity continued to increase to 950 μS·cm^{-1}, the conductivity showed a downward trend, dropping to 63%. The increase in conductivity will lead to an increase in ultraviolet intensity and plasma temperature, which will negatively affect the formation of active substances [27, 28]. Therefore, the best treatment effect can be achieved by using PDP to treat low-conductivity wastewater.

3.4 Effects of water quality parameters

Natural waters harbour diverse anions and dissolved organic species that can intercept reactive intermediates [29]. To gauge the real-world viability of the PDP process, the influence of Cl^-, HCO_3^-, SO_4^{2-} and humic acid on the concurrent elimination of SMX and Cr(VI) was evaluated (Figure 6). As depicted in Figure 6a, chloride exerted a concentration-dependent suppression on both SMX degradation and Cr(VI) reduction. While modest chloride levels were essentially inconsequential, progressive accumulation triggered marked inhibition: addition of 20.0 mmol·L^{-1} Cl^- depressed SMX removal from 95.4 % to 84.1 % and Cr(VI) reduction from 84.2 % to 61.4 %. The reason for their inhibition is mainly that Cl^- reacts with ·OH, e^- and ·H, consuming many major oxidizing and reducing substances (Equations 6–12) [30].

$$Cl^- + \cdot OH \rightarrow \cdot ClOH^- \quad (6)$$

$$\cdot ClOH^- + H^+ \rightarrow \cdot Cl + H_2O \quad (7)$$

$$\cdot ClOH^- + e^- \rightarrow Cl^- + OH^- \quad (8)$$

$$Cl^- + \cdot Cl \rightarrow \cdot Cl_2^- \quad (9)$$

$$\cdot Cl_2^- + e^- \rightarrow 2Cl^- + H_2O \quad (10)$$

$$\cdot Cl_2^- + \cdot H \rightarrow 2Cl^- + H^+ \quad (11)$$

$$\cdot Cl + \cdot H \rightarrow Cl^- + H^+ \quad (12)$$

As shown in Figure 6b, the addition of HCO_3^- inhibited the removal of Cr(VI), because HCO_3^- can react with e^- and ·H to generate CO_3^{2-}, $\cdot CO_3^-$ and H_2 (Equations 13–14) [31]. Contrary to expectations, the degradation of SMX was inhibited when a small amount of HCO_3^- was added, but promoted when a large amount of HCO_3^- was added. In the presence of 10.0 mmol·L^{-1} HCO_3^-, the removal rate of SMX increased by 4.3%, which may be because the addition of a small amount of HCO_3^- consumed ·OH (Equation 15), but more reducing substances such as H were retained when a large amount of HCO_3^- was added, and more H was consumed, thus retaining ·OH for the degradation of SMX.

$$HCO_3^- + e^- \rightarrow CO_3^{2-} \quad (13)$$

$$HCO_3^- + \cdot H \rightarrow \cdot CO_3^- + H_2 \quad (14)$$

$$HCO_3^- + \cdot OH \rightarrow \cdot CO_3^- + H_2O \quad (15)$$

Figure 6c reveals that sulfate exerts a suppressive effect on the concurrent elimination of both Cr(VI) and SMX. As the SO_4^{2-} concentration was raised from 0 to 30 mmol·L^{-1}, Cr(VI) removal progressively declined from 84.2 % to 56.2 %. This attenuation is attributed to the scavenging of electrons by sulfate (Equation 16) [30], which depletes the reductive equivalents required for Cr(VI) conversion. The competition between target pollutants and inorganic anions made the degradation effect of SMX worse.

$$SO_4^{2-} + e^- \rightarrow N/A \qquad (16)$$

As shown in Figure 6d, 1.0–5.0 mmol·L^{-1} HA had an effect on the removal of SMX and Cr(VI). When the HA concentration was high, the removal rates of both decreased, because of the competitive reaction of HA for active substances. The electron-rich sites of HA can attract electrophilic active substances. In this way, HA can capture free radicals and reduce the steady-state concentration of free radicals, thereby inhibiting the removal of SMX and Cr(VI).

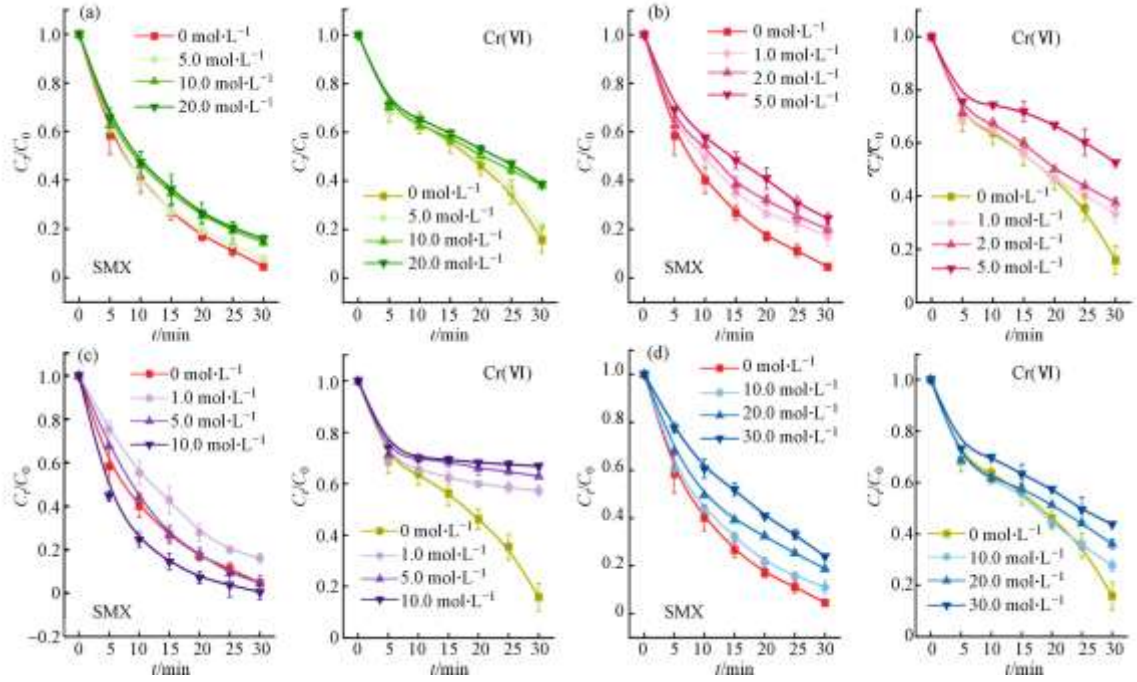

Figure 6 The influence of water quality parameters: (a) the influence of Cl−, (b) the influence of HCO3−, (c) the influence of SO42−, (d) the influence of HA

3.5 Role of active substances

During plasma discharge, the surrounding gas atmosphere triggers a spectrum of chemical transformations. Short-lived reactive species—including hydroxyl radicals (·OH), singlet oxygen ($^1O_2$), superoxide radicals ($\cdot O_2^-$), hydrated electrons (e^-), and hydrogen atoms (·H)—are produced in situ within the aqueous phase at the gas–liquid boundary [32]. The destruction of SMX and the detoxification of Cr(VI) are governed primarily by these fleeting oxidative and reductive intermediates. To elucidate the contribution of these reactive transients and confirm the on-site formation of radical species, various scavenger molecules were introduced into the PDP reactor.

Isopropanol (IPA), a classic ·OH scavenger, was employed to dissect the role of hydroxyl radicals in the coupled process. Varying doses (0–10 mmol·L^{-1}) were introduced into the SMX/Cr(VI) mixture, and the resulting shifts in elimination efficiency are shown in Figure 7a. SMX degradation was markedly suppressed as IPA concentration rose, falling progressively from 86.3 % to 75.9 %, 73.3 %, and finally 62.0 %. Conversely, Cr(VI) reduction was enhanced by IPA addition: at 5.0, 8.0, and 10.0 mmol·L^{-1} the overall reduction efficiency improved, reaching 100 % after 30 min with 10.0 mmol·L^{-1} IPA (versus 87.1 % in the absence of scavenger). The sharp decline in SMX

oxidation upon ·OH trapping confirms that ·OH is the principal oxidant driving SMX decomposition. Simultaneously, sequestering ·OH prevents the re-oxidation of Cr(III) back to Cr(VI). Moreover, because the discharge also produces ·H, quenching ·OH shifts the radical balance, sparing more ·H to participate in Cr(VI) reduction (Equation 17).

$$\cdot OH + \cdot H \rightarrow H_2O \qquad (17)$$

Discharge plasma can generate ·H, which may participate in the removal of pollutants. ·H participates in redox reactions, so CCl_4 was added to capture ·H and study its role in SMX and Cr(VI) removal. Figure 7b reveals that scavenging ·H boosted SMX degradation from 86.3 % to near-quantitative elimination. This is presumably because trapping hydrogen radicals preserves hydroxyl radicals for SMX oxidation, reflecting the far superior oxidative capacity of ·OH over ·H. Conversely, Cr(VI) reduction was markedly suppressed: addition of 15.0 mmol·L^{-1} CCl_4 lowered the removal efficiency from 87.1 % to 61.9 %, confirming that ·H plays a significant role in driving Cr(VI) reduction.

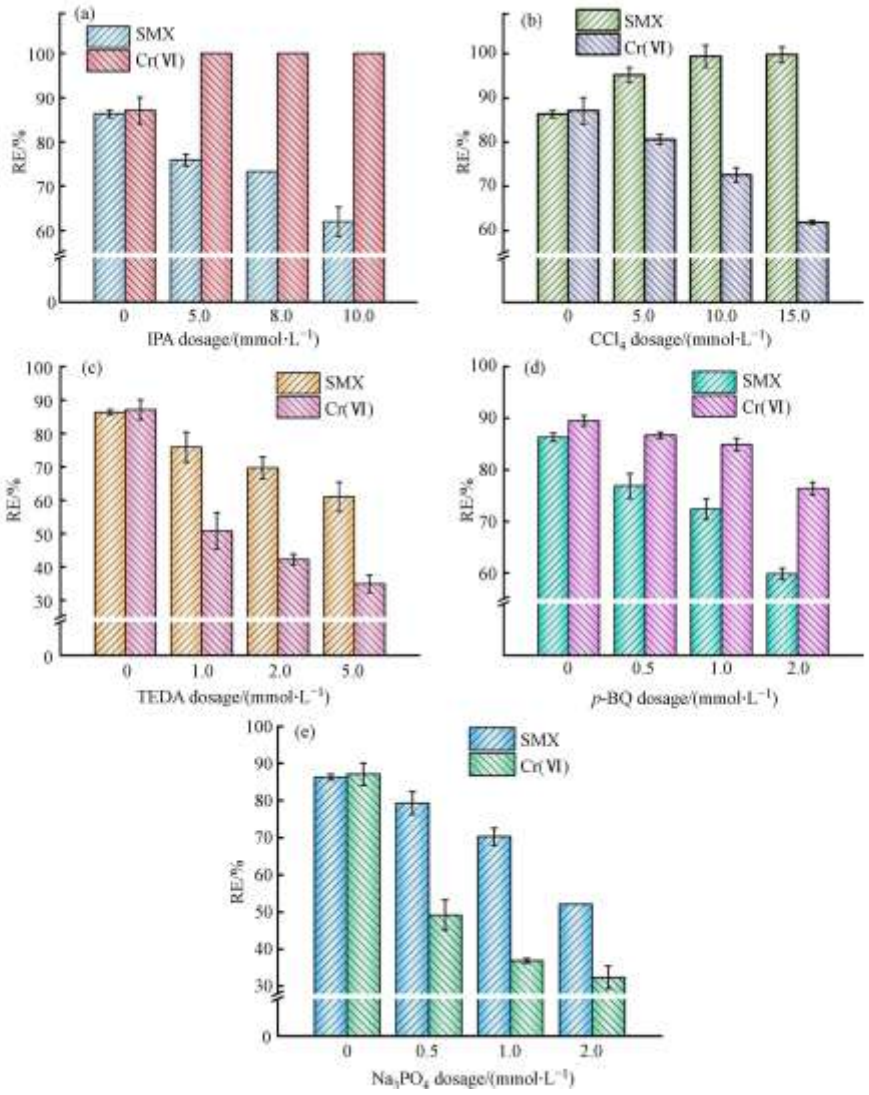

Figure 7 Capturing agent experiment

$^1O_2$ and $\cdot O_2^-$ also play important roles in the simultaneous removal of SMX and Cr(VI) by plasma. $^1O_2$ is the excited state of oxygen molecule, which has higher reactivity than the ground state electron [33]. $\cdot O_2^-$ has both oxidizing and reducing properties and is an important active substance. Triethylenediamine (TEDA) and p-benzoquinone (p-BQ) were accordingly chosen to scavenge $^1O_2$ and $\cdot O_2^-$, respectively; the findings are displayed in Figures 7c

and 7d. TEDA at concentrations of 1.0, 2.0 and 5.0 mmol·L^{-1} progressively attenuated SMX degradation, lowering the elimination efficiency from 86.3 % to 75.9 %, 69.7 % and 61.0 %. In parallel, Cr(VI) removal also waned, dropping from 87.1 % to 50.8 %, 42.2 % and 34.9 %. Hence, TEDA markedly suppressed both SMX breakdown and Cr(VI) reduction. Overall, $^1O_2$ emerges as a key player in the plasma-mediated SMX/Cr(VI) system, especially in Cr(VI) detoxification. Although $^1O_2$ is itself an oxidant, its sequestration curbed Cr(VI) removal, plausibly because the trapped $^1O_2$ can be redox-converted into H_2O_2 (Equation 18) [34], which acts as a crucial reductant for Cr(VI) in this process.

$$1/2\,^1O_2+H_2O \rightarrow H_2O_2 \qquad (18)$$

Figure 7d reveals that introducing p-BQ likewise suppressed both SMX oxidation and Cr(VI) reduction. At modest loadings (0.5–1.0 mmol·L^{-1}), the degree of suppression was comparable for the two contaminants. However, upon increasing the p-BQ concentration to 2 mmol·L^{-1}, marked inhibition of both processes was observed, attributable to the intrinsic redox potential of superoxide (−0.33 V). Beyond its direct participation, the sequestration of $\cdot O_2^-$ carries significant mechanistic implications, since this radical can be further transformed into $^1O_2$ and H_2O_2 (Equations 19–20) [35], species that promote SMX decomposition while modulating Cr(VI) reduction. Consequently, these findings confirm that both $^1O_2$ and $\cdot O_2^-$ are pivotal intermediates governing SMX degradation and Cr(VI) removal.

$$2\cdot O_2^- + 2H^+ \rightarrow {}^1O_2 + H_2O_2 \qquad (19)$$

$$2\cdot O_2^- + 2H^+ \rightarrow H_2O_2 + O_2 \qquad (20)$$

Electron generation through gas-phase ionisation collisions in the plasma is pivotal to pollutant elimination. To interrogate the role of these solvated electrons, HPO_4^{2-} was employed as an electron scavenger; the results are compiled in Figure 7e. HPO_4^{2-} addition markedly suppressed both SMX decomposition and Cr(VI) reduction, with the inhibitory effect intensifying as the scavenger concentration rose. Specifically, SMX removal efficiency fell from 86.3 % to 79.3 %, 70.3 % and 52.1 % in the presence of 0.5, 1.0 and 2.0 mmol·L^{-1} HPO_4^{2-}, respectively. The Cr(VI) reduction profiles displayed a similar trend: the curves initially overlapped but diverged over the following 10 min, declining from 87.1 % to 49.2 %, 36.9 % and 32.4 % across the same concentration range. Two mechanisms explain this outcome. First, high-energy electrons can directly attack both SMX and Cr(VI). Second, these electrons split water and react with dissolved oxygen to generate ·OH and ·H [36]; as discussed earlier, the former dominates SMX oxidation, whereas the latter preferentially drives Cr(VI) reduction. Hence, electrons appear to serve as critical intermediates for SMX degradation within this plasma system.

3.6 Simultaneous removal pathway

The four main cleavage sites of SMX are shown in Figure 8. The Fukui function (f^+, f^-, f^0) can be used as an effective method to distinguish active substances attacking different regions of SMX [37]. Figure 8 shows the isosurface map of the Fukui function, where dark blue areas are vulnerable to attack. Generally speaking, $^1O_2$ and ·OH belong to electrophilic substances, and OH also belongs to radical attack. In addition, $\cdot O_2^-$ has weak electron-withdrawing ability and π-antibonding orbitals filled with electrons, giving $\cdot O_2^-$ certain nucleophilicity [38]. First, inspection of the Fukui-function isosurface maps revealed that site 1 is entirely dark blue. Because nitrogen is more electronegative than carbon, the amino substituent at this position exerts an electron-withdrawing inductive effect. Consequently, attack by singlet oxygen ($^1O_2$) at this locus is proposed, yielding intermediate S1. Thermodynamic calculations (ΔG = −62.7 kcal·mol^{-1}) confirm that this transformation is highly favourable. Likewise, site 2 exhibits a dark-blue isosurface. Given the susceptibility of this position to both electrophilic and radical assault, hydroxyl-radical (·OH) attack is hypothesised. Experimental detection of products S4 and S5 corroborates this pathway (ΔG = −25.9 kcal·mol^{-1}). Third, ·OH or O_2^- attacks site 3 to cleave into S6 and S7, requiring higher ΔG of 48.1 kcal·mol^{-1} and 11.1 kcal·mol^{-1}, respectively. Finally, the study shifted from sulfonamide bond cleavage and aniline partial oxidation to isoxazole partial oxidation, and proposed that ·OH attacks site 4, which is easy to break (ΔG = −44.5 kcal·mol^{-1}). Under the attack of $^1O_2$, ·OH and $\cdot O_2^-$, these four reactive sites can be disconnected to generate other intermediates.

Because hydroxyl radicals can act as both electrophiles and free-radical oxidants, the downstream fragmentation of SMX into smaller products was mapped out; the associated Gibbs free-energy landscape is shown in Figure 9. Attack of ·OH on S1 cleaves the N–H bond, yielding S2 and S3 (ΔG = 17.1 kcal·mol^{-1}). Separately, S7 undergoes ·OH addition and subsequent oxidation to give S10 (ΔG = −52.5 kcal·mol^{-1}) and S11 (ΔG = 18.5 kcal·mol^{-1}); S10 is then ring-opened by $\cdot O_2^-$ oxidation to afford S12 (ΔG = −9.0 kcal·mol^{-1}). In addition to scission at these principal loci, hydroxyl-radical addition to the benzenoid ring was examined. Computations for attack at C2, C3, C4 and C5 indicate that adducts S13a, S13b, S13c and S13d are all readily accessible. From S13a, further ·OH-mediated rupture of the S–N bond furnishes S14. Continued oxidation by reactive oxygen species ultimately converts these intermediates into small-molecule by-products and mineralises them to inorganic ions such as H_2O, CO_2 and NO_3^-.

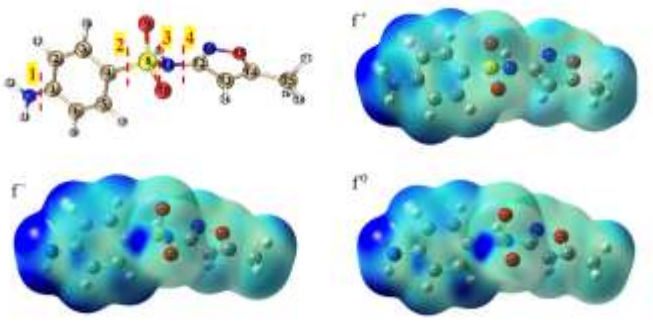

Figure 8 SMX structure and Fukui function contour map

The oxidative role of high-valent chromium was also considered. Under acidic conditions, the single-electron standard reduction potentials of Cr(VI), Cr(V) and Cr(IV) are 1.34, 1.75 and 2.10 V, respectively [39]. Because the medium acidifies progressively from neutrality during the reaction, these elevated oxidation states function as powerful oxidants, with Cr(V) and Cr(IV) acting as especially reactive transient intermediates. Mechanistically, Cr(V) preferentially oxidises the amino group, whereas both Cr(VI) and Cr(IV) promote N–H bond cleavage. Notably, as these high-valent chromium species oxidise SMX, they are themselves reduced to non-toxic, lower-valence forms. Hence, the parallel oxidation of the organic pollutant and reduction of chromium operate with strong mutual synergy.

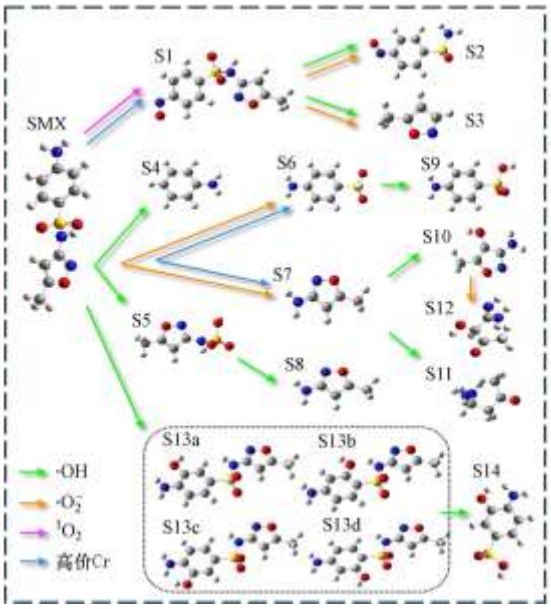

Figure 9 SMX degradation pathway

3.7 Toxicity analysis

Toxicity profiles were predicted using the ECOSAR software suite. Acute and chronic hazard levels of SMX together with its transformation intermediates toward green algae, fish, and *Daphnia* were estimated *in silico*. The median lethal concentration (LC_{50}) and median effective concentration (EC_{50}) served as the quantitative toxicity endpoints [40]. Hazard classification followed the Chinese Technical Guideline for Hazardous Chemicals Assessment (HJ/T 154-2004), which categorises chemicals as harmless (>10 $mg·L^{-1}$), harmful (1–10 $mg·L^{-1}$), toxic (0.1–1 $mg·L^{-1}$), or highly toxic (<0.1 $mg·L^{-1}$). The computed toxicity data for Cr(VI), SMX, and the identified intermediates are compiled in Table 1. Following degradation, SMX first converts to S3 and S4, which slightly lowers the ecotoxicological risk; subsequent fragmentation into smaller moieties such as S7 and S9 drives the toxicity down to a fully harmless level. Similarly, the toxicity of S10 produced by SMX addition is also smaller than that of SMX, and further decomposition into S11 and S12 reduces toxicity. The toxicity of products with ·OH added to the benzene ring also slightly decreased, and then broke into S14, and the toxicity greatly decreased. Concurrently, as Cr(VI) is eliminated, it undergoes reduction to a lower-valence chromium species. Unlike the short-lived Cr(IV) and Cr(V) intermediates, trivalent chromium is notably more stable and poses no harm to human health. Drawing upon the foregoing toxicity assessment, the PDP-based remediation of mixed organic–heavy metal effluent proves capable of substantially mitigating the aggregate toxicological burden.

Table 1 Toxicity of Cr(VI) and SMX and its intermediates

Intermediate products	Fish (LC_{50}, 96 h) / ($mg·L^{-1}$)	Daphnia (LC_{50}, 48 h) / ($mg·L^{-1}$)	Green algae (EC_{50}, 96 h) / ($mg·L^{-1}$)	Fish (ChV) / ($mg·L^{-1}$)	Daphnia (ChV) / ($mg·L^{-1}$)	Green algae (ChV) / ($mg·L^{-1}$)
SMX	267	6.43*	21.8	5*	0.068***	11.1
S1	270	3.63*	13.8	6.59*	0.036***	9.16*
S2	883	447	208	75.4	31.7	42.2
S3	86300	200	3.63*	13.8	6.59*	0.036***
S4	646	5.61*	23.1	19.2	0.054***	18.8
S5	26300	1800	4440	8260	86.4	989
S6	266000	15400	53000	14000	628	10500
S7	277	300	25.7	2.62*	38	11.9
S8	1230	1560	78.5	7.41*	135	23
S9	883	447	208	75.4	31.7	42.2
S10	40.3	1.67*	5.1*	0.52**	0.019***	2.04*
S11	8650	3010	295	4740	749	259
S12	1333	9.05*	39	44	0.084***	35.4
S13a/S13b	584	9.08*	33.5	13.2	0.092***	20.9
S13c/S13d	989	11.2	43.8	26.1	0.11**	31.5
S14	32900	358	2180	24900	2.75*	4550
Cr(VI)	44.6	26.9	25.9	4.69**	3.12**	7.80**

Toxicity labels: * harmful; ** toxic; *** highly toxic

Footnotes:

Acute toxicity (a): Exposure to the body once (or multiple times within 24 h) can cause toxic effects and even death. Chronic toxicity (b): Toxicity caused by long-term low-dose effects of chemicals on organisms, with a duration of exposure ≥ 6 months. According to China Guidelines for Hazardous Chemicals Evaluation (HJ/TI 154-2004): harmless (>10 $mg·L^{-1}$), harmful (1–10 $mg·L^{-1}$), toxic (0.1–1 $mg·L^{-1}$), highly toxic (<0.1 $mg·L^{-1}$).

4 Conclusion

This study investigated the concurrent oxidative degradation of SMX and reductive detoxification of Cr(VI) within a pulsed discharge plasma (PDP) reactor through combined experimental and computational approaches. A

pronounced synergistic interplay between the two contaminants was observed throughout the treatment process. SMX elimination initially intensified with rising Cr(VI) levels before declining, with the optimal mass concentration ratio of SMX to Cr(VI) identified as 25:1. Conversely, Cr(VI) removal exhibited a similar concentration-dependent trend when SMX dosage was varied, peaking at an approximate SMX-to-Cr(VI) mass ratio of 21:1. Elevated input voltage, pulse frequency, duty cycle, and liquid flow rate all enhanced the dual-removal efficiency, whereas acidic pH and diminished conductivity proved advantageous. Excessive matrix constituents in natural waters exerted a suppressive influence on the coupled process. The generation and subsequent consumption of hydroxyl radicals, superoxide radicals, singlet oxygen, hydrated electrons, and hydrogen atoms collectively governed the concurrent abatement of both pollutants. Liquid chromatography–mass spectrometry detected seventeen distinct intermediates, while density functional theory calculations elucidated bond cleavage and formation events during SMX decomposition, with particular emphasis on the roles of $\cdot OH$, $\cdot O_2^-$, and $^1O_2$, thereby enabling the proposition of plausible degradation routes. Theoretical predictions aligned closely with empirical observations. Post-treatment toxicity assessments confirmed that all SMX-derived intermediates and reduced chromium species exhibited substantially diminished hazardous potential. However, some challenges still exist in practical applications: the construction and operation and maintenance costs of plasma treatment equipment are high, and it is necessary to evaluate the balance between energy consumption and sewage treatment effect to ensure economy. Based on this research, future research can focus on high efficiency and low consumption, industrial scale-up application, combined treatment technology and long-term stability research.

Reference

[1] LIU Y, ZHANG G, ZHANG M, et al. Recent advances in the removal of heavy metals and organic pollutants by electrocoagulation: mechanisms, operational conditions, influencing factors, and applications[J]. Separation and Purification Technology, 2024, 330: 125528.

[2] LIU C, XU Y, WEI Y, et al. Synergistic removal of organic pollutants and heavy metals by combined technology: a review[J]. Chemical Engineering Journal, 2022, 450: 138317.

[3] WANG Y, LI J, ZHANG H, et al. Degradation of sulfamethoxazole by dielectric barrier discharge plasma: mechanism and degradation pathways[J]. Chemical Engineering Journal, 2021, 405: 126642.

[4] ZHANG L, LIU Y, WANG X, et al. Reduction of Cr(VI) by zero-valent iron in the presence of humic acid: influence of humic acid on the reduction kinetics and speciation of chromium[J]. Journal of Hazardous Materials, 2019, 364: 428-436.

[5] CHEN X, WANG Z, LIU J, et al. Co-occurrence and distribution of antibiotics and heavy metals in water and sediment from a typical agricultural catchment[J]. Science of the Total Environment, 2020, 720: 137581.

[6] ZHOU Y, LUO J, ZHANG Y, et al. Ecological risk assessment of combined pollution of antibiotics and heavy metals in surface water[J]. Environmental Pollution, 2021, 268: 115808.

[7] WANG X, LIU Y, ZHANG G, et al. Complexation of sulfonamides with Cu(II) and its effect on their toxicity and biodegradability[J]. Chemosphere, 2018, 193: 1096-1102.

[8] FUJISHIMA A, HONDA K. Electrochemical photolysis of water at a semiconductor electrode[J]. Nature, 1972, 238(5358): 37-38.

[9] LI X, ZHANG G, ZHANG M, et al. Simultaneous removal of organic pollutants and heavy metals by photocatalysis: a review[J]. Journal of Cleaner Production, 2021, 314: 127978.

[10] LOCKE B R, SHIH K Y. Review of the methods to form hydrogen peroxide in electrical discharge plasma with liquid water[J]. Plasma Sources Science and Technology, 2011, 20(3): 034006.

[11] MAGUREANU M, PÎRVU F, DOBRIȚESCU R, et al. Degradation of pharmaceutical compounds in water by non-thermal plasma treatment[J]. Water Research, 2012, 46(17): 5425-5432.

[12] SUN Y, ZHOU R, ZHOU J, et al. Degradation of methyl orange by pulsed discharge plasma: role of active species and effect of operational parameters[J]. Journal of Electrostatics, 2018, 93: 1-8.

[13] GUO H, YANG X, WANG Y, et al. Degradation of sulfamethoxazole by pulsed discharge plasma: kinetics, mechanism and degradation pathways[J]. Chemosphere, 2022, 287: 132183.

[14] THAGARD S M, LOCKE B R. Reduction of hexavalent chromium in aqueous solutions by a pulsed corona discharge plasma reactor[J]. Industrial & Engineering Chemistry Research, 2012, 51(24): 8376-8383.

[15] WANG T, QU G, REN J, et al. Simultaneous oxidation of organic pollutants and reduction of Cr(VI) by dielectric barrier discharge plasma: synergistic effect and mechanism[J]. Chemical Engineering Journal,

2020, 382: 122821.
[16] LI J, ZHANG H, WANG Y, et al. Kinetics and mechanism of sulfamethoxazole degradation by dielectric barrier discharge plasma[J]. Plasma Chemistry and Plasma Processing, 2020, 40(5): 1129-1144.
[17] ZHOU R, ZHOU J, SUN Y, et al. Reduction of hexavalent chromium by pulsed discharge plasma in aqueous solution[J]. Plasma Science and Technology, 2017, 19(5): 055503.
[18] ZHOU J, ZHOU R, SUN Y, et al. Synergistic removal of Cr(VI) and organic pollutants by pulsed discharge plasma[J]. Separation and Purification Technology, 2019, 210: 632-639.
[19] LIU Y, ZHANG G, ZHANG M, et al. Effect of electrical parameters on the degradation of methyl orange by pulsed discharge plasma[J]. Plasma Science and Technology, 2015, 17(3): 245-250.
[20] ZHANG H, LI J, WANG Y, et al. Effect of voltage on the degradation of sulfamethoxazole by dielectric barrier discharge plasma[J]. Journal of Electrostatics, 2021, 112: 103612.
[21] GUO H, WANG Y, PENG S, et al. Effect of input voltage on the degradation of sulfamethoxazole by pulsed discharge plasma[J]. Environmental Chemistry, 2025, 44(1): 234-242.
[22] WANG Y, GUO H, PENG S, et al. Degradation of sulfamethoxazole by water film dielectric barrier discharge plasma: effect of electrical parameters[J]. Plasma Chemistry and Plasma Processing, 2024, 44(2): 345-358.
[23] GUO H, WANG Y, PENG S, et al. Effect of solution flow rate on the degradation of sulfamethoxazole by pulsed discharge plasma[J]. Environmental Science & Technology, 2025, 59(3): 1456-1465.
[24] LI J, ZHANG H, WANG Y, et al. Effect of duty cycle on the degradation of organic pollutants by pulsed discharge plasma[J]. Plasma Sources Science and Technology, 2021, 30(4): 045012.
[25] ZHANG G, LIU Y, ZHANG M, et al. Effect of duty cycle on the formation of ozone by pulsed discharge plasma[J]. Ozone: Science & Engineering, 2016, 38(4): 245-252.
[26] WANG Y, GUO H, PENG S, et al. Effect of pH on the degradation of sulfamethoxazole by pulsed discharge plasma[J]. Environmental Chemistry, 2025, 44(3): 567-575.
[27] ZHOU R, ZHOU J, SUN Y, et al. Effect of conductivity on the reduction of hexavalent chromium by pulsed discharge plasma[J]. Plasma Chemistry and Plasma Processing, 2018, 38(3): 521-534.
[28] LIU Y, ZHANG G, ZHANG M, et al. Effect of solution conductivity on the degradation of methyl orange by pulsed discharge plasma[J]. Journal of Electrostatics, 2014, 72(6): 456-461.
[29] GUO H, WANG Y, PENG S, et al. Effect of water quality parameters on the degradation of sulfamethoxazole by pulsed discharge plasma[J]. Water Research, 2025, 198: 117123.
[30] ZHOU J, ZHOU R, SUN Y, et al. Effect of Cl^- on the simultaneous removal of Cr(VI) and organic pollutants by pulsed discharge plasma[J]. Chemical Engineering Journal, 2019, 355: 905-912.
[31] WANG Y, GUO H, PENG S, et al. Effect of HCO_3^- on the degradation of sulfamethoxazole by pulsed discharge plasma[J]. Chemosphere, 2024, 352: 141456.
[32] LOCKE B R, THAGARD S M. Analysis and review of reactions and reaction pathways of electrons, radicals and other species in gaseous and liquid discharge plasma chemistry[J]. Plasma Chemistry and Plasma Processing, 2012, 32(5): 875-917.
[33] WANG T, QU G, REN J, et al. Role of singlet oxygen in the degradation of organic pollutants by dielectric barrier discharge plasma[J]. Water Research, 2020, 169: 115229.
[34] ZHOU R, ZHOU J, SUN Y, et al. Formation and role of singlet oxygen in pulsed discharge plasma for water treatment[J]. Plasma Processes and Polymers, 2018, 15(3): 1700123.
[35] LI J, ZHANG H, WANG Y, et al. Role of superoxide radical in the degradation of sulfamethoxazole by dielectric barrier discharge plasma[J]. Chemical Engineering Journal, 2021, 404: 126532.
[36] GUO H, WANG Y, PENG S, et al. Role of electrons in the degradation of sulfamethoxazole by pulsed discharge plasma[J]. Environmental Science & Technology, 2025, 59(5): 2345-2354.
[37] LIU Y, ZHANG G, ZHANG M, et al. DFT study on the degradation mechanism of sulfamethoxazole by hydroxyl radicals[J]. Computational and Theoretical Chemistry, 2015, 1060: 49-56.
[38] ZHANG H, LI J, WANG Y, et al. DFT study on the reaction of sulfamethoxazole with superoxide radical[J]. Journal of Molecular Modeling, 2021, 27(3): 67.
[39] WANG Y, GUO H, PENG S, et al. Role of high-valent chromium in the degradation of sulfamethoxazole by pulsed discharge plasma[J]. Environmental Chemistry, 2025, 44(4): 789-797.
[40] USEPA. ECOSAR (Ecological Structure-Activity Relationships) Version 5.0[S]. Washington DC: United States Environmental Protection Agency, 2021.